J Low Temp Phys (2015) 178:18–34
DOI 10.1007/s10909-014-1220-7

Thermal Magnetoconductivity of Tungsten Below 6 K: Combining the Zero-, Low- and High-Field Cases

M. J. Hills · I. D. Hepburn · J. Bartlett · G. Hardy

Received: 11 April 2014 / Accepted: 27 August 2014 / Published online: 12 September 2014

Abstract We present a phenomenological expression to describe the thermal magnetoconductivity of tungsten which unifies the zero-field thermal conductivity with the low and high-field cases. Its basic form is derived from semi-classical magnetoresistance theory with fitting parameters allowing adjustment to particular samples. Thermal conductivity measurements at 5.5 K and in fields from 0 to 2 T are presented on two single crystals of tungsten with significantly different purities. We find that—with suitable adjustment of the fitting parameters—the equation is an excellent fit to the data in both cases. The significance of the fitting parameters and differences in their values are discussed, and we describe how they can be related to the individual properties of the samples. It is concluded that the equation should be applicable to any field below that at which orbit quantisation occurs and temperatures from 6 K down to tungsten's superconducting transition.

Keywords Tungsten · Thermal conductivity · Magnetoconductivity · Magnetoresistance · ADRs

Abbreviations

ADRs	Adiabatic demagnetisation refrigerators
PTR	Pulse tube refrigerator
RRR	Residual resistance ratio

M. J. Hills (✉) · I. D. Hepburn · J. Bartlett · G. Hardy
Mullard Space Science Laboratory, University College London, Holmbury St Mary, Dorking RH5 6NT, UK
e-mail: matthew.hills.11@ucl.ac.uk

1 Introduction

The magnetoresistive properties of tungsten have been studied since as early as the 1930s [1], motivated initially by the large magnitude and anisotropy of the effect in comparison with other metals. The majority of the work that followed took advantage of the ready availability of high-purity, single crystals to employ magnetoresistance measurements as a tool for probing tungsten's electronic structure [2,3]. These studies supported the detailed band structure calculations which had been performed on the transition metals [4,5]. Later investigations [6–9] looked in detail at the transport coefficients and scattering mechanisms at low temperature, and led to a largely successful attempt to use Fermi Surface data gathered from other sources to predict galvanomagnetic coefficients [10].

Although the majority of this past work focussed on electrical measurements, the thermal magnetoconductivity has also been studied [6,8,11] and the effect is found to be even larger than its electrical counterpart. This fact has attracted interest in the use of high-purity tungsten as a low temperature heat switch which might be applied in adiabatic demagnetisation refrigerators (ADRs) [12–15]. These refrigerators generally operate below 4 K and are one of the main technologies for accessing temperatures below the liquid helium regime. Cooling in an ADR is achieved by entropy reduction of an assembly of magnetic dipoles (typically in the form of a paramagnetic salt) through a cycle of magnetisation and subsequent demagnetisation. During magnetisation, the salt requires a good thermal link with a cold sink to dump the heat generated in this stage of the cycle, while during demagnetisation it must be thermally isolated from everything except the object to be cooled. A heat switch that exhibits a large "switching ratio" (i.e. the ratio of thermal conductivity in the "on" and "off" states) is therefore required. High switching ratios allow the heat generated during magnetisation to be extracted quickly, while ensuring a low parasitic heat load when the ADR is in the demagnetised state. Generally, ADRs already contain superconducting magnets capable of producing fields of several Tesla, which make incorporating a magnetoresistive switch relatively easy. Furthermore, the simplicity of such a switch offers great potential for miniaturisation of the cooler.

To facilitate the use of tungsten heat switches—in ADRs and other applications—it is critical to be able to predict its thermal conductivity from zero-field up to fields of several Tesla. Historically, it is only the high-field regime which has been studied and the behaviour at low fields has been given scant attention. For the case of ADR heat switches, this problem has been tackled by Canavan et al. [12], who proposed that the thermal magnetoresistance can be assumed to act in parallel with the zero-field resistance. This led them to formulate an expression for the thermal conductivity that covers all magnetic fields, thereby allowing them to estimate heat switch performance for the purposes of modelling. However, no detailed investigation was conducted to validate the expression.

In this paper, we show how such a combined expression may be arrived at from established semi-classical transport theory and that there is a basis for Canavan et al.'s assumption. We then report on thermal conductivity tests at 5.5 K, in fields of 0–2 T, on two different tungsten crystals, which demonstrate how well the theoretical equation fits the measured behaviour.

2 Theory

Thermal currents in tungsten, in common with any metal, are carried by two mechanisms: the movement of "hot" electrons down a thermal gradient and "cold" electrons up it; and by phonons carrying thermal energy from the "hot" to the "cold" regions. At the temperatures we are concerned with in this paper (<6 K), the phonon contribution to the heat current is at least 4 orders of magnitude smaller than the electronic contribution [11]. Furthermore, it is not affected by the presence of the magnetic field. For these reasons our theoretical approach focuses primarily on the electronic part of the thermal conductivity and exploits the similarity of its behaviour in a magnetic field to its electrical counterpart.

Semi-classical transport theory provides a framework for explaining the magnetoresistive properties of metals in both low and high-fields [16]. The distinction between "low" and "high" fields is made using the quantity $\omega_c\tau$, where $\omega_c$is the cyclotron frequency and τ is the relaxation time. A metal is normally said to be in the "high-field" condition when $\omega_c\tau >> 1$. Following Pippard [16], we interpret $\omega_c\tau$ as the mean angle turned by an electron between collisions and make the more precise definition for the high-field condition, $\omega_c\tau \geq 2\pi$—i.e. the applied field is such that an electron can complete one or more orbits about the axis of the magnetic field before being scattered. Furthermore, we assume that the field is not sufficient to cause orbit quantisation effects, such as are associated with the *Shubnikov-de Haas* effect and other oscillatory phenomena.

In the low-field case, solutions are found to the transport equations using power series expansions in magnetic field, **B**, and these then lead to a form for the conductivity which is a similar expansion [17]. In the high-field case, electrons complete one, or more, real-space orbits and the corresponding **k**-space orbits are constrained to surfaces of constant energy. The resulting effects on transport properties are determined by the shape of these energy surfaces (the Fermi Surface). The theory in this case [18,19] also leads to conductivities which are power series expansions in **B**, with retention of only the first non-vanishing term deemed necessary for sufficient accuracy of calculation [19]. For the case of transverse magnetoconductivity considered here (where the thermal current and the measured thermal gradient are in the same direction, which is perpendicular to the magnetic field) both the low and high-field theories predict a conductivity which varies as $1/B^2$.

The governing equation for conduction problems, with and without the presence of a magnetic field, is the Boltzmann equation [20]:

$$\left.\frac{\partial f_k}{\partial t}\right]_{\text{diff}} + \left.\frac{\partial f_k}{\partial t}\right]_{\text{field}} + \left.\frac{\partial f_k}{\partial t}\right]_{\text{scatt}} = 0 \tag{1}$$

This tells us that, in steady state, the change in the distribution of electron states f_k caused by diffusion, external fields and scattering, respectively, must balance. In the general case, where temperature gradients and electric and magnetic fields may be present, the equation takes the following form [20,21]:

$$-\mathbf{v_k}\cdot\frac{\partial f_k}{\partial T}\nabla T - \frac{e}{\hbar}(\mathbf{E}+\mathbf{v_k}\times\mathbf{B})\cdot\frac{\partial f_k}{\partial \mathbf{k}} = -\left.\frac{\partial f_{\mathrm{k}}}{\partial \mathrm{t}}\right]_{\text{scatt}} \tag{2}$$

Here e and $\mathbf{v}_k$ are the electron unit charge and velocity, respectively, T is the temperature, $\hbar$ is the reduced Planck constant, $\mathbf{E}$ and $\mathbf{B}$ are the electric and magnetic fields and $\mathbf{k}$ is the electron wave vector.

Rather than express the right-hand side of Eq. (2) using a complete collision integral [22], we use the well-known *relaxation time* approximation [20]:

$$-\left.\frac{\partial f_k}{\partial t}\right]_{\text{scatt}} = \frac{f_k - f_k^0}{\tau} = \frac{g_k}{\tau} \tag{3}$$

i.e. the "out-of-balance" part of the electron distribution g_k decays exponentially on removal of the applied fields according to a characteristic relaxation time τ:

$$-\frac{\partial g_k}{\partial t} = \frac{g_k}{\tau} \tag{4}$$

So that

$$g_k(t) = g_k(0)\exp(-t/\tau) \tag{5}$$

Although this is a simplified phenomenological description of the real processes at work, it is generally considered a reasonable approximation when scattering is catastrophic and there is evidence that it produces realistic results for tungsten [10]. It is likely to be a good assumption at low temperatures when impurities and electron-electron interactions are the dominant scattering mechanisms. Our measurements of the temperature dependence of tungsten's conductivity appear to back up this assumption [Hepburn et al. in preparation], which is further reinforced by the findings of others [8,11].

The implicit assumption in using the relaxation time approach is that the scattering probability per unit time, P, is proportional to the reciprocal of the relaxation time [23]:

$$\frac{1}{\tau} \propto P \tag{6}$$

Now, as we are seeking an equation which covers the zero-field to high-field conditions and everything in between, we postulate the following: an electron will be scattered either by mechanisms which limit the zero-field conductivity (with probability P_0) *or* by the mechanisms that modulate the high-field conductivity (with probability P_B) and that these two mechanisms are independent. To find the total probability of an electron being scattered we simply sum these two effects:

$$P_{\text{tot}} = P_0 + P_B \tag{7}$$

This could equivalently be formulated in terms of Matthiessen's rule:

$$\frac{1}{\tau} = \frac{1}{\tau_0} + \frac{1}{\tau_B} \tag{8}$$

Here we have associated a relaxation time with the part of the conductivity which varies in a magnetic field. This idea has been used before [24], where it was argued

that one could equate the reversal of an electron's motion due to the Lorentz force with a scattering event. We make no claim that such a direct physical interpretation is valid, but merely use it as a phenomenological mechanism to deal with conductivities over a wide range of fields.

If a **k** independent relaxation time is assumed for each mechanism, each reciprocal of relaxation time, $1/\tau$, can be associated with a resistivity due to that mechanism [23] and we can write directly:

$$\rho = \rho_0 + \rho_B \tag{9}$$

i.e.

$$\frac{1}{\kappa_e} = \frac{1}{\kappa_0} + \frac{1}{\kappa_B} \tag{10}$$

where we have subsequently converted the resistivities to conductivities and κ_e is the electronic part of the thermal conductivity. For the purposes of comparison, we note here that the more rigorous approach of solving the Boltzmann equation using the variational principle leads to $\rho \geq \rho_0 + \rho_B$ [22].

For temperatures below 6 K the zero-field thermal conductivity as a function of temperature is found to be well represented by [11],

$$\frac{1}{\kappa_0(T)} = \frac{a_1 + a_2 T^2}{T} \tag{11}$$

where a_1 and a_2 are fitting parameters. If they are interpreted according to established transport theory [22], then they represent contributions from impurity and electron-electron scattering, respectively.

High-field measurements on tungsten [9] have shown that, below 6 K, κ_B, as a function of temperature, can be fitted to

$$\kappa_B(T) = \frac{a_3 T + a_4 T^4}{B^n} \tag{12}$$

where B is the magnetic field and a_3, a_4 and n are fitting parameters. Semi-classical magnetoresistance theory predicts a value of 2 for n [18,25], although deviations from this have been observed for tungsten [2,6,26,27].

Substituting (11) and (12) into Eq. (10) and re-arranging we have

$$\kappa_e(T) = \frac{1}{\frac{a_1 + a_2 T^2}{T} + \frac{B^n}{a_3 T + a_4 T^4}} \tag{13}$$

At this point we include a term for the lattice conductivity, which we assume to be acting in parallel to the electronic thermal conductivity. The lattice conductivity in tungsten has been found to be proportional to T^2 [9,11], giving for the complete thermal conductivity:

$$\kappa(T) = b_0 T^2 + \frac{1}{\frac{a_1 + a_2 T^2}{T} + \frac{B^n}{a_3 T + a_4 T^4}} \tag{14}$$

where b_0 is the phonon conductivity coefficient. Equation (14) describes the behaviour of the thermal conductivity of tungsten below 6 K as a function of magnetic field and temperature, and is in agreement with the expression of Canavan et al. [12].

In this paper, we test Eq. (14) at constant temperature. For this case, all terms which are functions of T become constant and the expression may be simplified to

$$\kappa = b_l + \frac{1}{\frac{1}{\kappa_0} + \frac{B^n}{a}} \tag{15}$$

where κ_0 is the electronic part of the zero-field conductivity and both a and b_l are fitting parameters. Equation (15) is the expression used to fit the data presented below.

3 Experimental Details

To test the validity of Eq. (15), thermal magnetoconductivity measurements were made on two very different single crystal tungsten samples. The samples had significantly different purities (see Table 1) and were chosen to demonstrate that Eq. (15) would apply for different levels of impurity scattering. The details of both samples are given below.

The first sample (Fig. 1) was cut from a zone-refined rod such that the length of interest for the measurements was in the [100] direction (see Fig. 3). The short length of the sample, combined with its high purity, meant that it was not possible to measure its electrical resistance at 4 K and therefore the Residual Resistance Ratio (RRR = resistance at 300 K/resistance at 4.2 K) could not be determined. However, other samples from the same supplier with similar thermal conductivities had RRR values of over 100,000. This will be referred to hereafter as sample C-3b.

The second sample was cut—from a less pure single crystal—into a more complex shape to maximise the free length for heat switch applications (see Fig. 2). The crystal was grown in the [111] direction and then cut so that the free length was in the plane perpendicular to this direction (see Fig. 3). The sample's RRR was measured as 580 ± 65. Thermometers were placed such that the temperature difference was measured over a length of 82 mm.

Table 1 Sample details

Sample	Supplier	Dimensions	RRR	Crystal orientation
C-3b	Metal Crystals and Oxides Ltd[a] (Cambridge, UK)	1.55 mm × 1.37 mm × 5.9 mm long	>100,000	[100] direction along sample length (∥ to heat flow) (see Fig. 3)
M-2.2	MaTecK[b] (Juelich, Germany)	2.22 mm × 2.12 mm × 82 mm long	600	[111] ∟ to plane containing the sample length (see Fig. 3)

[a] www.metal-crystals.com
[b] www.mateck.com

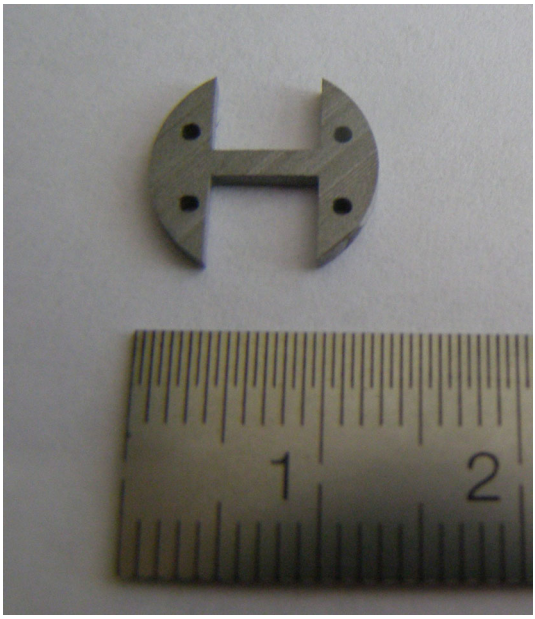

Fig. 1 The high-purity tungsten sample (C-3b) Colour figure online

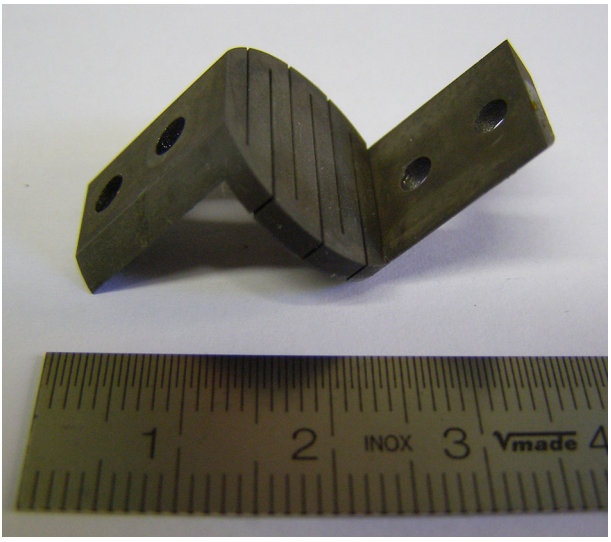

Fig. 2 The lower purity tungsten sample (M-2.2) Colour figure online

The samples were mounted in a cryogen-free cryostat, cooled by a Cryomech Pulse Tube Refrigerator (PTR), and oriented such that the direction of heat flow between the thermometers would be perpendicular to the magnetic field, which was provided by a 2 T, 2A superconducting magnet. For the low-field measurements, this was powered from a Cryogenic power supply that permitted current control to ± 1 mA, whereas

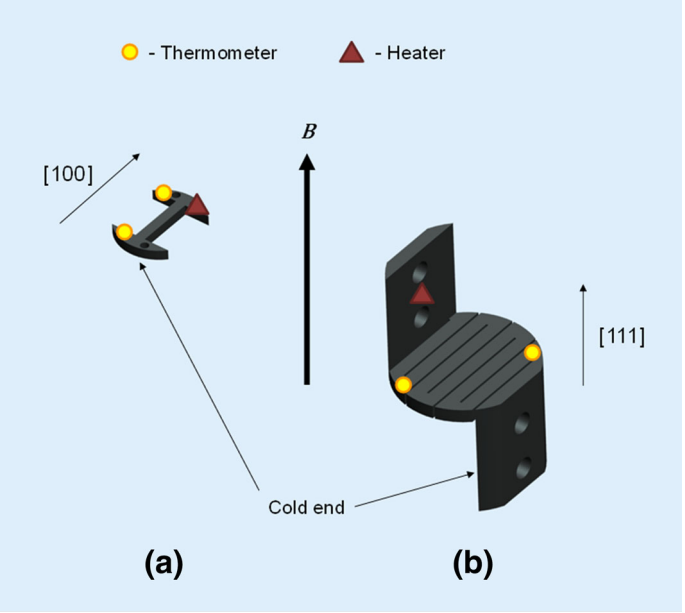

Fig. 3 Measurement set-up showing relative orientations of the sample, the applied magnetic field and known crystal axes **a** Sample C-3b, **b** Sample M-2.2 Colour figure online

for fields of >0.1 T current was provided by a Thurlby Thandar power supply with a precision of ± 10 mA. The true current flowing in the magnet was measured separately on a Fluke ammeter.

In order to measure the thermal conductivity, one end of the sample was fixed to the cold stage of the PTR. Cernox thermometers were mounted at each end of the length of interest of the sample, as shown in Fig. 3, and these were used to measure the temperature difference (ΔT) created by passing current through a heater (10 kΩ resistor) mounted to the free end. The thermal conductivity was measured by recording the steady-state temperature difference between the thermometers for a given heater power. To improve measurement statistics, the thermometers were read by taking the output from an AVS-47 resistance bridge into an Agilent nanovoltmeter and using this to average a 30 s sample (with readings taken at approximately 2.5 Hz $\approx$ 75 readings). Two separate measurements were made for each heater power and magnetic field combination, and the temperature differences were averaged. The thermal conductivity was then calculated according to

$$\kappa = \frac{Q}{\Delta T}\frac{L}{A} \tag{16}$$

with Q being the supplied power, L the sample length and A the area.

All measurements were performed at 5.5 K with a temperature stability of ± 0.05 K achieved by servo control of the PTR. At this temperature the PTR had sufficient cooling power to absorb the heat input required to achieve a measureable ΔT of $\sim$250 mK.

3.1 Errors

The following sources of error were considered when calculating the vertical error bars in the figures: errors in the thermometer readings, errors in the measured voltage and current in the heater, and errors in the measured sample dimensions. Errors in the temperature readings were the averaged standard deviations of the 30 s samples read out by the nanovoltmeter. Being of the order of 5–10 mK, these were much larger than errors due to the thermometer calibration fits (1–2 mK) and self-heating effects (∼20 pW), which were consequently both neglected. No account was made for magnetoresistive effects in the thermometers, although previous research suggests this will be less than 1 % for the temperatures and fields in this study [28,29]. Current and voltage errors were assumed to be of the same order as the resolutions of the respective meters. The sample dimensions were measured at room temperature, but any change in size due to thermal contraction would only be a small fraction of ±20 μm errors assumed for the cross section dimensions and the ±50 μm error assumed for the sample lengths.

Of the sources of error mentioned above, by far the most dominant were errors in the measured ΔT—these ranging from approximately 5 % to more than 25 % for the lowest field measurements on sample C-3b. The same errors in sample M-2.2 were always below 5 % because the longer sample length enabled larger ΔTs and proportionally smaller errors. Errors in measured heater power ranged from less than 0.5 % to around 5 %; however, the largest errors were at the highest fields (when the smallest powers were used), so that there was no coincidence of large power errors and large ΔT errors. By comparison to the other errors, those in the measured samples dimensions were small, being less than 1 % in length and less than 3 % in area.

As is evident from the figures, total errors are larger in the lower field measurements, where the temperature differences are smaller. However, by taking advantage of averaging at least two readings for each data point, they are reduced to less than 15 % in all but the lowest fields.

Horizontal error bars in the figures indicate the error in the measured field, taken to be either 0.001 or 0.01 T depending on the power supply being used.

4 Results and Discussion

The results for sample C-3b are shown in Figs. 4 and 5; those for sample M-2.2 are shown in Figs. 6 and 7. The fits were made using chi-square minimisation to Eq. (15). The parameter values for the fits are summarised in Table 2.

The figures illustrate that Eq. (15) is an excellent fit to the thermal magnetoconductivity of both samples. As described in Sect.2, Eq. (15) combines a lattice conductivity (b_l) with a zero-field electrical conductivity (k_0) and a field-dependent electrical conductivity (a/B^n). The magnitudes of these elements of the conductivity are plotted in Figs. 8a and 9a, which illustrate how they vary with magnetic field. For sample C-3b, the field-dependent conductivity has become less than the zero-field electrical term at 0.005 T, whilst in sample M-2.2 the crossover does not occur until 0.05 T. The figures make clear that the main cause of this is the difference in the k_0 term: it is

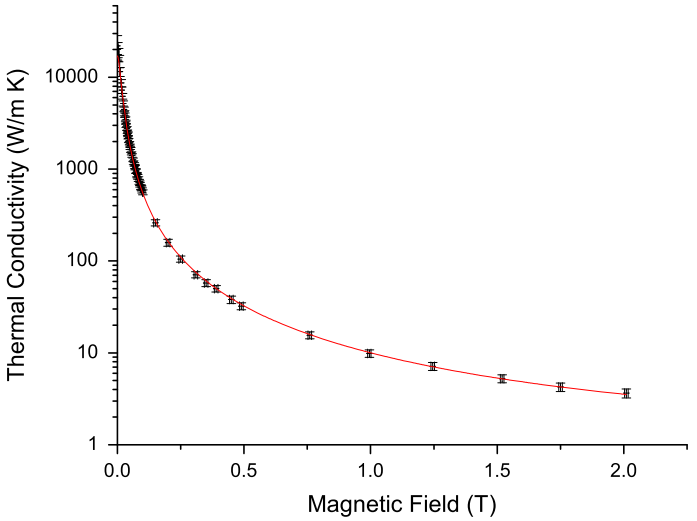

Fig. 4 Magnetoconductivity of sample C-3b from 0 to 2 T. The fitted curve is to Eq. (15) (Colour figure online)

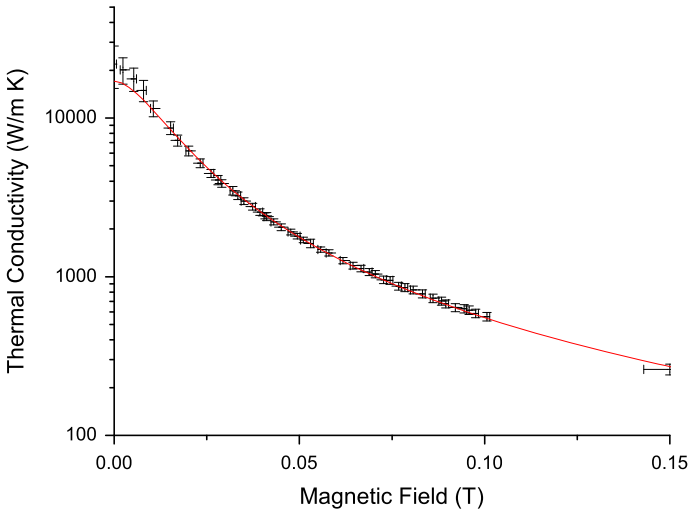

Fig. 5 Low-field (0–0.15 T) magnetoconductivity of sample C-3b. The fitted curve is to Eq. (15) (Colour figure online)

more than an order of magnitude larger for sample C-3b—a reflection of the higher purity of this sample. Figure 8a shows that the lattice term is the smallest contribution in sample C-3b, even at the highest fields. Note that the lattice contribution for sample M-2.2 is not shown in Fig. 9 as, within the errors of the fits, b_l was found to be zero (see Table 2). Figures 8b and 9b show the percentage contribution from the different elements of the conductivity. The difference in the field at which the field-dependent component drops below the zero-field electrical component is clear from these figures

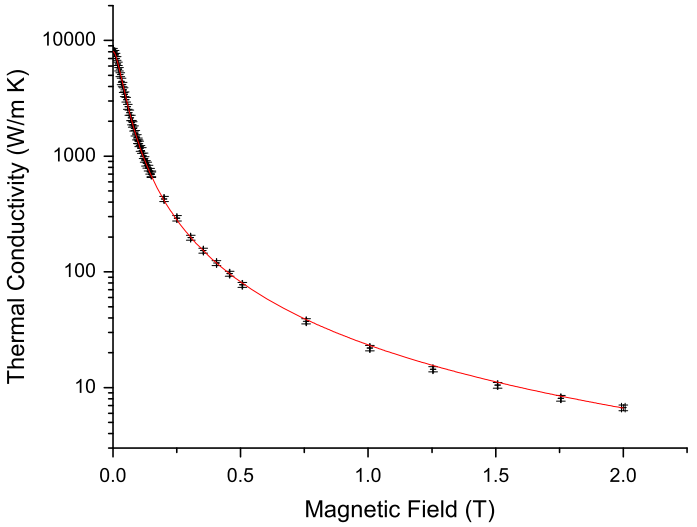

Fig. 6 Magnetoconductivity of sample M-2.2 from 0 to 2 T. The fitted curve is to Eq. (15) (Colour figure online)

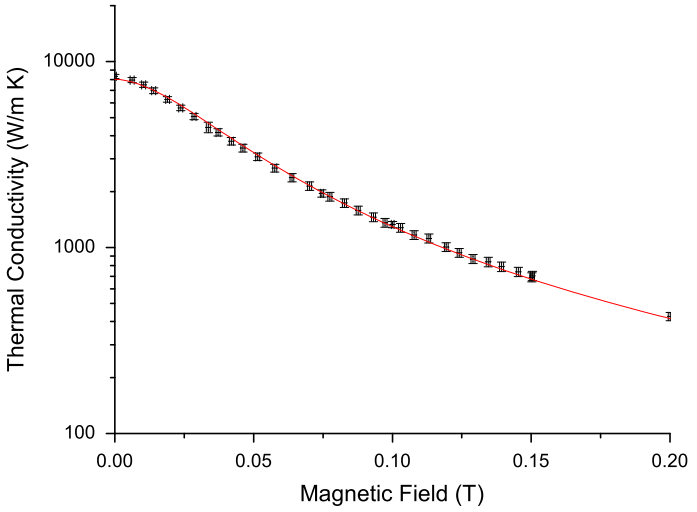

Fig. 7 Low-field (0–0.2 T) magnetoconductivity of sample M-2.2. The fitted curve is to Eq. (15) (Colour figure online)

too. There is also a more rapid drop in the field-dependent contribution for sample C-3b compared to sample M-2.2 because of the smaller a term; this is discussed in more detail below.

The chi-square minimisation produces different fitting parameters for each sample and these will be described in turn. The lattice conductivity in sample M-2.2 is found to be zero with the fitting error of ± 0.30, compared to 0.93 ± 0.16 for sample C-3b. The results of others [9,11] suggest that b_l can be approximated by $0.05\,\mathrm{T}^2$ W/m K.

Table 2 Comparison of fitting parameters for the two samples

Sample	b_l	κ_0(measured)	κ_0(fitted)	n	a	Adjusted R-square[a]
C-3b	0.93 ± 0.16	$21{,}920 \pm 6{,}530$	$17{,}085 \pm 642$	1.80 ± 0.01	9.11 ± 0.19	0.99923
M-2.2	0 ± 0.30	$8{,}333 \pm 223$	$8{,}032 \pm 84$	1.82 ± 0.01	23.48 ± 0.48	0.99895

[a] Used as a measure of the goodness of fit; the closer this value to 1, the better the fit. It is calculated as $\overline{R}^2 = 1 - \frac{\mathrm{RSS}/\mathrm{df}_{\mathrm{Error}}}{\mathrm{TSS}/\mathrm{df}_{\mathrm{Total}}}$, where RSS is the residual sum of squares, TSS is the total sum of squares about the mean, $\mathrm{df}_{\mathrm{Total}}$ is the total number of degrees of freedom (=($n-1$) where n is the sample size) and $\mathrm{df}_{\mathrm{Error}} = (n-p-1)$ where p is the number of parameters in the fitting expression

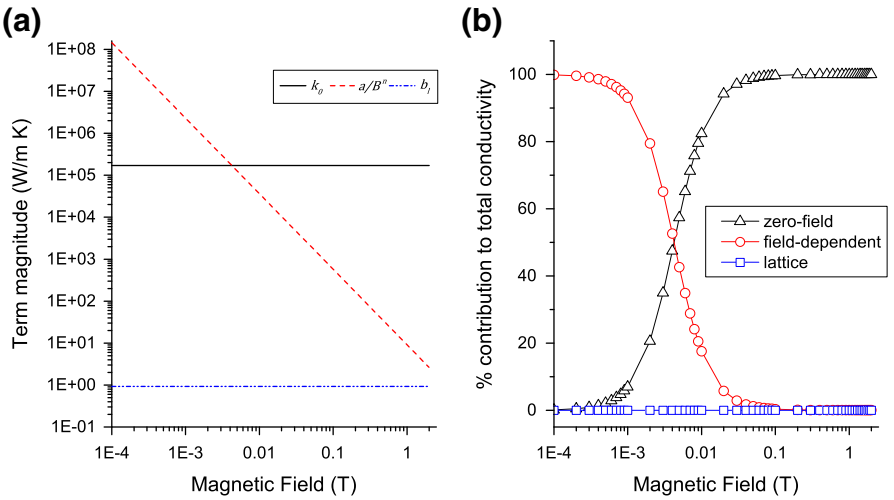

Fig. 8 Relative contributions of the lattice, zero-field electrical and field-dependent parts of Eq. (15) for sample C-3b plotted as **a** absolute magnitudes and **b** percentages of the total conductivity (Colour figure online)

Using this with T = 5.5 K yields a value of 1.51, which is greater than the b_l value in both our fits. It is unlikely that there is no phonon contribution at all. However, it may be that the phonon current is restricted by the geometry of our samples. Scattering from the sample surface could act to destroy the phonon current, particularly in the case of sample M-2.2 because the convoluted geometry forces a phonon that travels the whole sample length to interact with the surface. A theoretical treatment of phonon scattering at surfaces [22] indicates that scattering will be diffuse when the phonon wavelength is significantly smaller than the typical asperity height on the surfaces. It can be shown that this is likely to be the case in our samples by calculating the wavelength corresponding to the peak in the phonon energy spectrum. Assuming a Debye distribution, the frequency at which the peak occurs is given by [30]:

$$\omega_{\max} \approx \frac{2.82 k_B T}{h} \tag{17}$$

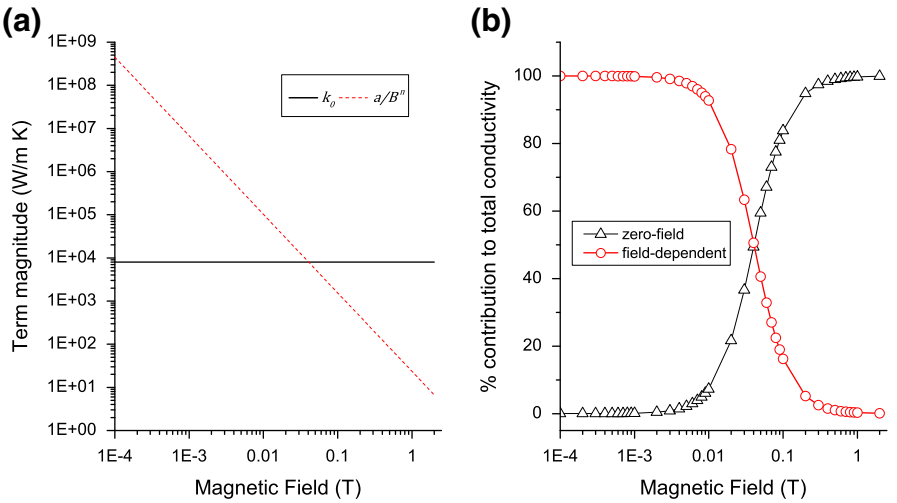

Fig. 9 Relative contributions of the lattice, zero-field electrical and field-dependent parts of Eq. (15) for sample M-2.2 plotted as **a** absolute magnitudes and **b** percentages of the total conductivity (Colour figure online)

where k_B is the Boltzmann constant and h is Planck's constant. Calculating this for T = 5.5 K, yields $\omega_{max} = 3.23 \text{ x } 10^{11} \text{s}^{-1}$, which can then be converted to a wavelength using the speed of sound in tungsten, v_w :

$$\lambda_{\omega_{\max}} = \frac{2\pi v_w}{\omega_{\max}} \tag{18}$$

If the speed of sound in tungsten is taken—from high frequency mechanical resonance measurements [31]—as approximately 2,900 m/s, we find $\lambda_{\omega_{\max}} \cong 0.06\,\mu\text{m}$. Surface asperities this small would be difficult to achieve in a carefully polished sample and our crystals were not subject to such preparation. On this basis, it is entirely possible that surface scattering plays an important role in limiting the phonon current and may explain why it is smaller in the case of M-2.2.

The difference in the zero-field conductivities (κ_0) is as would be expected for two samples of such differing purities. The values from both fits agree with the measured zero-field conductivities of the samples to within the measurement errors: $21{,}920 \pm 6{,}530$ W/m K for sample C-3b and $8{,}333 \pm 223$ W/m K for sample M-2.2. The larger error on the measured zero-field conductivity of sample C-3b is the result of only being able to generate a small ΔT without raising the base temperature of the apparatus (a consequence of the sample's short length and high conductivity).

There is good agreement between fits for the magnetic field exponent (n). As noted above, semi-classical magnetoresistance theory leads us to expect a value of 2. However, deviations from this that are of the same order as we observe have been seen by Long [6], Canavan et al. [12], Marchenkov et al. [26] and Cherepanov et al. [27]. Long attributes his value to an appreciable (field independent) lattice conductivity, but this would be at odds with the minimal lattice contribution we find in our fits. It also seems

inconsistent with tungsten's relatively high Debye temperature (400 K [30]). Canavan et al. merely note that the deviation from $n = 2$ is surprising without offering further explanation. Marchenkov et al. [26], on the other hand, present a physical mechanism related to the difference they observe in the exponent when the current is directed along different crystal axes. They suggest that at certain temperatures, there will be phonons of an appropriate wavevector to scatter electrons from one Fermi surface sheet to a nearby point on an adjacent one. The sizes of the gaps between sheets in **k**-space depend on the plane in which the electrons are moving. For certain crystal orientations, this intersheet scattering then permits some electron orbits to become open, or extended, even though the energy surfaces themselves are closed. The presence of some open orbits changes the predictions of semi-classical magnetoconductivity theory significantly: for orientations in which these orbits play a role in conduction, the electrical part of the thermal conductivity is expected to saturate at a constant value as B approaches infinity [16]. In other words, the conductivity becomes independent of B at high-fields and n tends towards zero. In their experiments, Marchenkov et al. [26] only see this effect become significant at temperatures above 30 K although, given a Debye phonon distribution, there is no reason why it should not be seen at lower temperatures.

Quasi-open orbits may arise from another source: namely the Static Skin Effect [32]. This effect has been studied extensively [32,33] and it has been shown that when the Larmor radius (r_B) of electrons (i.e. the radius of the electron orbits) is significantly smaller than the sample dimension perpendicular to the magnetic field, the majority of the electron transport takes place in a layer of approximately the same thickness as the Larmor radius next to the surface. This is because electrons reflected from the surface (either specularly or diffusely) are much more likely to progress along the sample than those in the bulk, which make multiple orbits before scattering and are hence constrained to travel no further than the Larmor radius. The Larmor radius can be calculated using the following equation.

$$r_B = \frac{mv}{eB} \tag{19}$$

Here, m, e and v are the electron mass, charge and velocity, respectively; B is the magnetic field. Using standard values for the mass and charge of a free electron and a typical value for the Fermi velocity of an electron in tungsten ($\approx 5 \times 10^5$ m/s [34]), we find that r_B in our samples varies between approximately 6×10^{-2} mm at $B = 0.05$ T and 1.4×10^{-3} mm at $B = 2$ T—i.e. several orders of magnitude smaller than the sample dimensions. This, taken together with the fact the electron mean free paths for our samples in the absence of magnetic field are likely to be much greater than these values, satisfies the conditions for the Static Skin Effect [33].

When incident and reflected electrons at a surface are correlated, with just the component of momentum perpendicular to the sample surface being reversed, they can be said to be specularly reflected. Electrons interacting in this way are able to move to a different Fermi surface sheet, creating an open trajectory. These open orbits may then contribute to a change in n on the same basis as described above for intersheet scattering. Some initial results from a study by Volkenshtein et al. [35] suggested that

when sample faces specularly reflect a high proportion of electrons (approximately 60 %) the magnetoresistance contains an additional linear component. However, in a fuller report on their findings [33], they conclude that a magnetic field exponent of 1.96 ± 0.05 fits their data for samples with both specularly and diffusely reflecting surfaces.

A separate, but connected, surface effect that may also be present in our samples is the influence of lattice defects just below the surface [27]. Our crystals were spark-eroded to their final geometry and were not subject to any polishing or other surface treatment. As a result, we might expect some level of damage to the crystal structure in the vicinity of the sample surface. Lattice defects arising in this way can penetrate hundreds of microns into the sample [27] and thus encompass the region of the sample where most of the electron current is present under the Static Skin Effect. Cherepanov et al. [27] studied the impact of this on the magnetoresistance through high-field measurements on spark-eroded crystals which satisfied the conditions for the Static Skin Effect: they measured the transverse magnetoresistance for samples after spark eroding and again after they had been electro-polished to remove the defect layer. Polishing caused the magnetic field exponent to increase from 1.34 to 1.98, indicating that sub-surface defects were responsible for a reduction in the magnetic field exponent. We believe that this is the most likely cause of the fact that we find a magnetic field exponent of less than 2. The mechanism for the change is discussed in more detail by Kolesnichenko [36]; it is related to the fact that the increased scattering in the defect layer causes the magnetoresistance to depend not just on the applied field, but on the electron mean free path in the layer and the layer's thickness. Kolesnichenko derives an expression for the change in transverse conductivity that contains two terms: the first includes the Larmor radius squared (and is hence proportional to $1/B^2$, by equation (19)), while the second is a function of the product of the thickness of the defect layer and the mean free path of the electrons in this layer [36]. The implication is that the change in conductivity can no longer be expected to be a simple function of $1/B^2$.

Lastly, the different values of a can be interpreted as a reflection of the different levels of impurity scattering in the two samples. Wagner [9] shows that an expression for a, derived according to semi-classical theory, is of the same form as the theoretical expression for the zero-field thermal resistivity found by solving the Boltzmann equation using the variational method [37]. As illustrated by Eq. (11), this is expected—and it has been confirmed experimentally [11]—to contain a $1/T$ term, which can be associated with the impurity scattering. This term will increase with greater impurity scattering (i.e. lower sample purity and RRR) and the a value in our fits seems to follow this general trend, being significantly larger for the lower purity sample M-2.2.

5 Conclusions

We have proposed an equation to describe the thermal magnetoconductivity of tungsten from zero- to high-field conditions drawing on the principles of semi-classical transport theory. This equation has been tested against results from two very different single crystals of tungsten and has been shown to be an extremely good fit to the

data in both cases. Our measurements cover a sufficient range of fields to include regions where the high-field conductivity contribution dominates and where the low-field contribution dominates. The magnetic fields associated with these regions differ between the samples due to their differing purities. We are thus able to conclude that our fit works well in both low-field and high-field regions and that it handles differing sample impurities well through appropriate adjustment of the κ_0 and a parameters. The magnetic field dependence of the electronic part of the thermal conductivity is not—as one might expect from semi-classical transport theory—precisely quadratic. We believe the most likely cause of this to be lattice defects in the sub-surface layer resulting from spark eroding the samples. We find a minimal phonon contribution to the thermal conductivity in our fits and suggest that this may be the result of surface scattering.

The data presented in this paper confirm the applicability of Eq. (14) at 5.5 K and between 0 and 2 T. Nevertheless, we also expect it to work equally well at any temperature below 6 K (down to tungsten's superconducting transition at approximately 10 mK [38]) and at any magnetic field below that at which electron orbit quantisation occurs. Its validity at lower temperatures will be the subject of a future publication.

Acknowledgments M. J. H. acknowledges the support of a Science & Technology Facilities Council (STFC) studentship. I. D. H. acknowledges support from STFC (Grant numbers ST/H00260X/1 and STK000977/1) and the Engineering and Physical Sciences Research Council (EPSRC grant number EP/H04888X/1). We would like to thank one of the referees for their helpful comments on the importance of surface effects in interpreting our results.

References

1. E. Justi, H. Scheffers, Phys. Z. **37**, 700 (1936)
2. E. Fawcett, Phys. Rev. **128**, 154 (1962)
3. E. Fawcett, W.A. Reed, Phys. Rev. A **134**, 723 (1964)
4. W.M. Lomer, Proc. Phys. Soc. **80**, 489 (1962)
5. L.F. Mattheiss, Phys. Rev. A **139**, 1893 (1965)
6. J.R. Long, Phys. Rev. B **3**, 1197 (1971)
7. J.R. Long, Phys. Rev. B **3**, 2476 (1971)
8. D.K. Wagner, J.C. Garland, R. Bowers, Phys. Rev. B **3**, 3141 (1971)
9. D.K. Wagner, Phys. Rev. B **5**, 336 (1972)
10. J.R. Long, Phys. Rev. B **3**, 1209 (1971)
11. A.B. Batdalov, N.A. Red'ko, Sov. Phys Solid State **22**, 664 (1980)
12. E.R. Canavan, M.J. Dipirro, M. Jackson, J. Panek, P.J. Shirron, J.G. Tuttle, in *Advances in Cryogenic Engineering* (American Institute of Physics, 2002), pp. 1183–1190
13. J.-M. Duval, B.M. Cain, P.T. Timbie, in *Proceedings of SPIE*, ed. by J. Zmuidzinas, W.S. Holland, S. Withington (2004), pp. 802–811
14. J.-M. Duval, B.M. Cain, P.T. Timbie, AIP Conf. Proc. **710**, 1729 (2004)
15. J. Bartlett, G. Hardy, I. Hepburn, R. Ray, S. Weatherstone, Cryogenics **50**, 647 (2010)
16. A.B. Pippard, *Magnetoresistance in Metals* (Cambridge University Press, Cambridge, 1989)
17. L. Davis, Phys. Rev. **56**, 93 (1939)
18. I.M. Lifshitz, M.I. Azbel, M.I. Kaganov, Sov. Phys. JTEP **4**, 41 (1957)
19. E. Fawcett, Adv. Phys. **13**, 139 (1964)

20. J.M. Ziman, *Principles of the Theory of Solids*, 2nd edn. (Cambridge University Press, Cambridge, 1972)
21. A.H. Wilson, *The Theory of Metals*, 2nd edn. (Cambridge University Press, Cambridge, 1954)
22. J.M. Ziman, *Electrons and Phonons* (Oxford University Press, New York, 1960)
23. N.W. Ashcroft, D.N. Mermin, *Solid State Physics* (Holt-Saunders International, Tokyo, 1981)
24. S. Olszewski, Acta Phys. Pol. A **120**, 525 (2011)
25. M.I. Azbel, M.I. Kaganov, I.M. Lifshitz, Sov. Phys. JTEP **5**, 967 (1957)
26. V.V. Marchenkov, A.N. Cherepanov, V.E. Startsev, C. Czurda, H.W. Weber, J. Low Temp. Phys. **98**, 425 (1995)
27. A.N. Cherepanov, V.V. Marchenkov, V.E. Startsev, N.V. Volkenshtein, M. Glin'skii, Sov. J. Low Temp. Phys. **12**, 666 (1986)
28. G. Heine, W. Lang, Cryogenics **38**, 377 (1998)
29. B.L. Brandt, D.W. Liu, L.G. Rubin, Rev. Sci. Instrum. **70**, 104 (1999)
30. C. Kittel, H. Kroemer, *Thermal Physics* (W. H Freeman and Company, New York, 2000)
31. D.I. Bolef, J.D. Klerk, J. Appl. Phys. **33**, 2311 (2004)
32. V.G. Peschanskii, M.Y. Azbel, Sov. Phys. JTEP **28**, 1045 (1969)
33. N.V. Volkenshtein, M. Glin'skii, V.V. Marchenkov, V.E. Startsev, A.N. Cherepanov, Sov. Phys. JETP **68**, 1216 (1989)
34. J. Kollár, Solid State Commun. **27**, 1313 (1978)
35. N.V. Volkenshtein, V.V. Marchenkov, V.E. Startsev, A.N. Cherepanov, M. Glin'skii, JETP Lett. **41**, 458 (1985)
36. Y.A. Kolesnichenko, Sov. J. Low Temp. Phys. **11**, 641 (1985)
37. F.J. Blatt, *Physics of Electronic Conduction in Solids* (McGraw-Hill Book Company, New York, 1968)
38. J.W. Gibson, R.A. Hein, Phys. Rev. Lett. **12**, 688 (1964)